Virtual synchronous control of brushless doubly-fed induction generator

Min Lu, Yefei Zhang, Xinhong Cai, Hui Li*

Shihezi University, Shihezi 832000, China

cqulh@163.com

ABSTRACT. *This paper attempts to provide inertia contribution of wind turbines in the access to weak grid with low short-circuit ratio. To this end, a virtual synchronous control (VSC) was presented for brushless doubly-fed induction generator (BDFIG) based on the popular phase-locked loop synchronizing technique. The VSC-BDFIG can synchronise with the grid directly through active power control and differs from other VSC controls in the imitation of the operation features and inner potential-control winding current relation of synchronous generator. Then, an electromechanical motion equation was established to describe the inertial dynamics of VSC-BDFIG wind turbines. Thanks to the imitation of the operation features of synchronous generator, the BDFIG naturally provides the desired inertial response like synchronous generator. Later, the frequency response features of a single wind turbine were simulated at different controller parameters and operation conditions. The results verify the superiority of the VSC-BDFIG on inertial support capability and operation stability over the typical phase-locked loop-based vector control, especially for weak grid access. The research findings shed new light on the application of the BDFIG in wind power systems.*

RÉSUMÉ. *Cet article tente de fournir une contribution d'inertie des éoliennes dans l'accès à un réseau faible avec un faible rapport de court-circuit. À cette fin, un contrôle virtuel synchrone (VSC) a été présenté pour le générateur à la cascade hyposynchrone Brushless(BDFIG), basé sur la technique populaire de synchronisation au circuit fermé. Le VSC-BDFIG peut se synchroniser directement avec le réseau via un contrôle de puissance actif et diffère des autres contrôles VSC par l'imitation des caractéristiques de fonctionnement et la relation de courant d'enroulement de contrôle de potentiel interne du générateur synchrone. Ensuite, une équation de mouvement électromécanique a été établie pour décrire la dynamique inertielle des éoliennes VSC-BDFIG. Grâce à l'imitation des caractéristiques de fonctionnement du générateur synchrone, le BDFIG fournit naturellement la réponse inertielle souhaitée comme un générateur synchrone. Plus tard, les caractéristiques de réponse en fréquence d'une seule éolienne ont été simulées pour différents paramètres du contrôleur et conditions de fonctionnement. Les résultats confirment la supériorité du VSC-BDFIG sur la capacité de support inertiel et de la stabilité de fonctionnement sur le contrôle vectoriel basé sur un circuit fermé typique, en particulier pour un accès faible au réseau. Les résultats de la recherche apportent un nouvel éclairage sur l'application du BDFIG dans les systèmes éoliens.*

KEYWORDS: *brushless doubly-fed induction generator (BDFIG), hidden inertia, virtual synchronous control (VSC), wind turbine.*

MOTS-CLÉS: générateur à la cascade hyposynchrone brushless (BDFIG), inertie cachée, contrôle synchrone virtuel (VSC), éolienne.

DOI:10.3166/EJEE.20.115-132 © 2018 Lavoisier

1. Introduction

With the proliferation of wind power worldwide, the intermittency and randomness of wind have posed new challenges to the adequacy and stability of large-scale wind power grids (Ackermann, 2005; Eirgrid, 2011). There are mainly two types of grid stability: the transient stability and the small-signal stability. The former refers to the recoverability from big disturbances and the latter, that from small disturbances. The small-signal stability is fundamental to power grids, owing to the ubiquitous presence of small disturbances.

Doubly-fed inductor generator (DFIG) is commonly implemented in power grids, thanks to its variable speed constant frequency (VSCF) control. In the DFIG, the frequency is regulated by the machine-side convertor (MSC). However, the frequency-speed relation is described by hidden inertia, which does not apply to frequency or voltage and affects the grid stability. To solve the problem, much research has been done to control the hidden inertia (Arani and EI-Saadany, 2013; Shuai *et al*., 2016), the droop (Solanki *et al.*, 2016), the pitch angle and the harmonies (Jauch *et al.*, 2007).

As a typical DFIG, the brushless doubly-fed induction generator (BDFIG) can realize reliable and low-cost VSCF control with the dual-stator mechanism. The structure of the BDFIG is illustrated in Figure 1 below. This type of DFIG is also featured by hidden inertia, due to the vector control based on phase-locked loop.

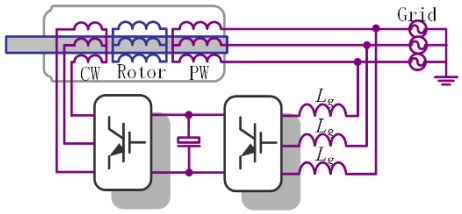

Figure 1. BDFIG structure

To eliminate the hidden inertia, ELECTRICA, together with nine western European institutions, introduced virtual synchronous control (VSC) to add virtual rotational inertia to wind turbines or photovoltaic motors (Gorginpour *et al*., 2013). Zhong and M. Rezalravani presented a VSC plan of voltage source control, which supports micro-grid mode and seamless switch between grid-tie and isolated operation. Yuko Hirase puts forward the mechanical equation of the rotor and the voltage equation of the stator for synchronous generator according to the external feature and

mechanism of the generator (Lv *et al.*, 2014). Considering the variation of input power with the operation points, initial conditions and pitch angles, Hu et al. integrated the VSC theory into DFIG control to reflect the frequency variation and form the hidden inertia (Wang *et al.*, 2015).

The above studies reveal that the VSC helps to prevent the negative impacts of hidden inertia on the frequency and stability of large wind power grids. Of course, different control strategies have different interface circuits, despite following the same VSC principle. Overall, the current VSC theorists emphasize on grid-connected inverter, DFIG and grid-connected circuit over the BDFIG, although the latter has been well applied in wind power systems.

To make up for the research gap, this paper puts forward a novel VSC strategy for the BDFIG that mimics the operation mode of synchronous generators. The imitation marks the main contribution of our research. The proposed strategy was validated through a simulation. The remainder of this paper is organized as follows: Section 2 introduces the models of synchronous generator and the BDFIG; Section 3 presents the detailed designs of the VSC of the BDFIG; Section 4 analyses the small-signal modelling and stability of VSC-BDFIG; Section 5 verifies the effect of the proposed VSC strategy through simulation; Section 6 wraps up this research with some valuable conclusions.

2. Models of synchronous generator and the BDFIG

As mentioned before, this section introduces the models of synchronous generator and the BDFIG. Note that the generator convention was adopted in the stator, while motor convention in the rotor.

2.1. Model of synchronous generator

The grid stability can be expressed as a two-stage model:

$$\begin{aligned} v_s &= -R_s i_s + s\varphi_s + j\omega_s \varphi_s \\ \varphi_s &= -L_s i_s + L_{ad} i_f \end{aligned} \tag{1}$$

where vs, is, φ_s and if are stator voltage vector, stator current vector, stator flux vector and rotor current vector, respectively. The rotor flux voltage can be expressed as:

$$\begin{aligned} v_f &= R_f i_f + L_f s i_f \\ \varphi_f &= L_f i_f - L_{ad} i_s \end{aligned} \tag{2}$$

where vf and φ_f are rotor voltage vector and rotor flux vector, respectively.

The electrical torque balance can be expressed as:

$$T_m - T_e - D\Delta\omega_r = J\frac{d\omega_r}{dt} \tag{3}$$

where Tm is the input mechanical torque; Te is the electromagnetic torque; D is the inherent damping coefficient; J is the physical equivalent inertia constant; ωr is the rotor speed.

2.2. BDFIG model

$$v_p = -R_p i_p + s\varphi_p + j\omega_p\varphi_p \tag{4}$$

$$\varphi_p = -L_p i_p + L_{s1r} i_r \tag{5}$$

$$v_c = -R_c i_c + s\varphi_c + j(\omega_p - (p_1 + p_2)\omega_r)\varphi_c \tag{6}$$

$$\varphi_c = -L_c i_c + L_{s2r} i_r \tag{7}$$

$$v_r = R_r i_r + s\varphi_r + j(\omega_p - p_1\omega_r)\varphi_r \tag{8}$$

$$\varphi_r = L_r i_r + L_{s1r} i_p + L_{s2r} i_c \tag{9}$$

where vp, vc and vr are the voltage vectors of power winding, control winding and rotor winding, respectively; ip, ic and ir are the current vectors of the three windings, respectively; φ_p, φ_c, φ_r and are the flux vectors of the three windings, respectively; ω_p is the speed of power winding. The ω_p is equivalent to the ω_{grid} under the grid-connection mode.

3. VSC for BDFIG

3.1. Synchronous generator features under grid voltage orientation

Since the synchronous generator model is aligned with the grid voltage frame, we have:

$$v_{ds} = v_{grid} \tag{10}$$

$$v_{qs} = 0 \tag{11}$$

Then, equation (1) can be rewritten as:

$$v_s = -R_s i_s - L_s s i_s + e_0 \tag{12}$$

where the e_0 is the inner potential of synchronous generator.

$$e_0 = L_{ad} s i_f + j\omega_s(-L_s i_s + L_{ad} i_f) \tag{13}$$

According to equations (12) and (13), the terminal voltage depends on the inner potential of the stator of synchronous generator, and the magnitude of e_0 hinges on the magnitude of rotor flux φ_f. Since the inner potential is always orthogonal to φ_f, the angular frequency of e_0 equals that of φ_f.

3.2. BDFIG features under grid voltage orientation

Since the BDFIG model is aligned with the grid voltage frame, we have:

$$v_{pd} = v_{grid} \tag{14}$$

$$v_{pq} = 0 \tag{15}$$

Substituting equation (5) into equation (4), we have:

$$v_p = -R_p i_p - L_p s i_p + L_{s1r} s i_r + j\omega_p(L_p i_p + L_{s1r} i_r) \tag{16}$$

The control winding current can be controlled directly, but not rotor current. Considering equations (8) and (9), we have:

$$\begin{aligned} v_p = & -R_p i_p - (L_p - L_{s1r} k_1) s i_p \\ & + \underbrace{L_{s1r} k_2 s i_c - j\omega_p (L_p - L_{s1r} k_1) i_p + j\omega_p L_{s1r} k_2 i_c}_{e_{0\_B}} \end{aligned} \tag{17}$$

where $k_1 = \frac{L_{s1r}}{L_r}, k_2 = \frac{L_{s2r}}{L_r}$

3.2.1. Imitation of inner potential

The similarity between equations (12) and (17) indicates that the power winding voltage of the BDFIG can be expressed in a similar form with that of synchronous generator, and that e_{0_B} is controlled by the control winding current i_c produced by the MSC. Comparing the two equations, it is clear that the inner potential terms must be the same to imitate the inner potential of synchronous generator, that is, $e_{0\_B}=e_0$. The imitation is depicted in Figure 2(b), where the blue dashed box represents the inherent physical structure of the BDFIG.

According to Figure 2(b) and equation (17), the inner potential e_0 of the BDFIG can be expressed as:

$$e_0 = \underbrace{(L_{s1r}k_2 s + j\omega_p L_{s1r}k_2)}_{G_x} i_c - \underbrace{(j\omega_p (L_p - L_{s1r}k_1))}_{G_y} i_p \tag{18}$$

The control winding current can be expressed as:

$$i_c = \frac{1}{G_x} e_0 + \frac{G_y}{G_x} i_p \tag{19}$$

Therefore, the BDFIG can be controlled similarly to synchronous generator by equation (19).

3.2.2. Imitation of impedance

Comparing equations (12) and (17), it can be seen that the two expressions only differ in impedance. The virtual impedance should be introduced to imitate the impedance of synchronous generator:

$$e_{vir} = (R_{vir} + sL_{vir}) i_p \tag{20}$$

where R_{vir} is the virtual resistance; L_{vir} is the virtual reactance; evir is the virtual potential vector.

The power winding voltage of the BDFIG can be expressed as:

$$\begin{aligned} v_p - (e_0 + e_{vir}) &= [R_p + s(L_p - L_{s1r}k_1)] i_p + (R_{vir} + L_{vir}) i_p \\ &= (R_s + sL_s) i_s \end{aligned} \tag{21}$$

Thus, we have:

$$\begin{aligned} R_{vir} &= R_p - R_s \\ L_{vir} &= (L_p - L_{s1r}k_1) - L_s \end{aligned} \tag{22}$$

Since the above control strategy cannot directly control the power winding current ip, it is necessary to convert this current into the control winding current i_c. According to equations (20)~(22), we have:

$$G_z = \frac{R_{vir} + sL_{vir} + G_y}{G_x} \tag{23}$$

where Gz is the function to transfer i_p into i_c.

3.2.3. Control loop for control winding current

The control loop for control winding current was adopted to adjust the control winding current. The reference current of control winding was obtained from the e0 of synchronous generator and virtual impedance. Considering equations (21), (23) and (24), the virtual potential can be expressed as:

$$i_c^* = \underbrace{\frac{1}{G_x}}_{Part\ 1} e_0 + \underbrace{\frac{G_z G_y}{G_z G_x + G_y}}_{Part\ 2} i_p \tag{24}$$

The two parts of the above equation are the term related to the input e_0 and the cross coupling term. Substituting equations (18) and (23) into equation (24), we have:

$$i_c^* = \underbrace{\frac{1}{L_{s1r}k_2 s + j\omega_p L_{s1r}k_2}}_{G1} e_0 + \underbrace{[\frac{(R_{vir}+sL_{vir})j\omega_p(L_p - L_{s1r}k_1) + [j\omega_p(L_p - L_{s1r}k_1)]^2}{(R_{vir}+sL_{vir})(L_{s1r}k_2 s + j\omega_p L_{s1r}k_2) + 2j\omega_p(L_p - L_{s1r}k_1)(L_{s1r}k_2 s + j\omega_p L_{s1r}k_2)}]}_{G2} i_p \tag{25}$$

The differential terms can be ignored because the synchronous generator has a much slower time scale than the BDFIG. Thus, equation (25) can be rewritten as:

$$i_c^* = \underbrace{\frac{1}{j\omega_p L_{s1r}k_2}}_{G1} e_0 + \underbrace{[\frac{-\omega_p(L_p - L_{s1r}k_1)^2 + j(R_{vir}+sL_{vir})(L_p - L_{s1r}k_1)}{-2\omega_p L_{s1r}k_2(L_p - L_{s1r}k_1) + jL_{s1r}k_2(R_{vir}+sL_{vir})}]}_{G2} i_p \tag{26}$$

Equation (26) is the rule for the current controller of the BDFIG.

The d-q axis can be described by equation (20):

$$i_{cd}^* + ji_{cq}^* = \underbrace{\frac{1}{\omega_p L_{s1r}k_2}}_{G1} e_{0q} - j\underbrace{\frac{1}{\omega_p L_{s1r}k_2}}_{G1} e_{0d} + \underbrace{[\frac{{\omega_p L_{ps}}^2 2\omega_p L_{s1r}k_2 L_{ps} + (R_{vir}+sL_{vir})^2 L_{ps}L_{s1r}k_2}{(2\omega_p L_{s1r}k_2 L_{ps})^2 + [L_{s1r}k_2(R_{vir}+sL_{vir})]^2} +}_{G2} \underbrace{j\frac{-2\omega_p L_{s1r}k_2 L_{ps}^2(R_{vir}+sL_{vir}) + \omega_p {L_{ps}}^2 L_{s1r}k_2(R_{vir}+sL_{vir})}{(2\omega_p L_{s1r}k_2 L_{ps})^2 + [L_{s1r}k_2(R_{vir}+sL_{vir})]^2}]}_{G3}(i_{pd} + ji_{pq}) \tag{27}$$

Then, we have:

$$\begin{cases} i_{cd}^{*} = G_1 e_{0q} + (G_2 i_{pd} - G_3 i_{pq}) \\ i_{cq}^{*} = -G_1 e_{0d} + (G_2 i_{pq} + G_3 i_{pd}) \end{cases} \tag{28}$$

(4) Equivalent electric inner potential

$$\begin{aligned} e_{0\_B} &= G_1 i_c - G_2 i_p = \left| e_{0\_B} \right| e^{j\theta_p} \\ &= \left| e_{0\_B} \right| e^{j(\theta_{ctr} + \theta_{PLL})} \end{aligned} \tag{29}$$

where $e_{0\_B} = \sqrt{e_{0\_Bd}^2 + e_{0\_Bq}^2}; \theta_{ctr} = aectan \frac{e_{0\_Bq}^2}{e_{0\_Bd}^2}$.

Then, we have:

$$\begin{aligned} \Delta e_{0\_B} &= \frac{e_{0\_Bd0}}{\sqrt{e_{0\_Bd0}^2 + e_{0\_Bq0}^2}} \Delta e_{0\_Bd} \\ &\quad + \frac{e_{0\_Bq0}}{\sqrt{e_{0\_Bd0}^2 + e_{0\_Bq0}^2}} \Delta e_{0\_Bq} \\ &= \frac{e_{0\_Bd0}}{e_{0\_B0}} \Delta e_{0\_Bd} + \frac{e_{0\_Bq0}}{e_{0\_B0}} \Delta e_{0\_Bq} \end{aligned} \tag{30}$$

3.3. VSC-BDFIG model

Through the above analysis, the author proposed the VSC-BDFIG (Figure 2) that operates as a synchronous generator through the imitation of inner potential and virtual impedance. The model of synchronous generator consists of electrical and mechanical equations. The input torque by the controller of synchronous generator T_m can be expressed as:

$$T_m = k_{p\_SG}(\omega_r^{*} - \omega_r) + k_{I\_SG} \int (\omega_r^{*} - \omega_r) dt \tag{31}$$

where ω_r^{*} equals the speed of grid, i.e., $\omega_r^{*} = \omega_{grid}$; k_{p_SG} and k_{I_SG} are the PI controller parameters of the controller.

Then, the total electromagnetic torque Te can be expressed as:

$$T_e = \varphi_{ds} i_{qs} - \varphi_{qs} i_{ds} = -L_s i_{ds} i_{qs} + L_f i_f i_{qs} + L_s i_{qs} i_{ds} \tag{32}$$

In light of equations (1)~(9), (31) and (32), the VSC-BDFIG model can be established as:

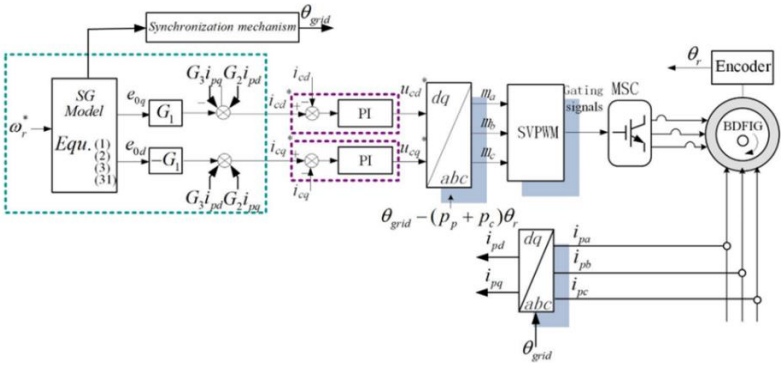

Figure 2. Schematic diagram of the VSC-BDFIG

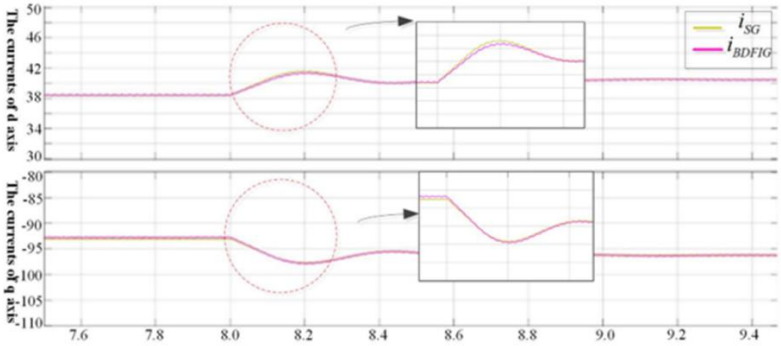

Figure 3. The d-q axis current waves of the synchronous generator and the BDFIG

$$\begin{cases} v_s = -R_s i_s - L_s s i_s + e_0 \\ v_f = R_f i_f + L_f s i_f \\ Js\omega_r = k_p(\omega_{grid} - \omega_r) + k_I \int (\omega_{grid} - \omega_r)dt \\ \quad -(-L_d i_{ds} i_{qs} + L_f i_f i_{qs} + L_q i_{qs} i_{ds}) - D\Delta\omega_r \\ s\theta = \omega \\ v_p = -R_p i_p - (L_p - L_{s1r} k_1) s i_p + e_0 \\ v_c = k_{p\_B}(i_c^* - i_c) + k_{I\_B} \int (i_c^* - i_c)dt \end{cases} \tag{33}$$

The control plan of the model is shown in Figure 2.

4. Small-Signal Modelling and Stability Analysis of the VSC-BDFIG

4.1. Simulation of synchronous generation imitation

Section 3 shows that the VSC-BDFIG can totally mimic the synchronous generator. The imitation ability is verified through simulation in this section on a test platform with a synchronous generator and a VSC-BDFIG. The two generators are connected to the same grid and share the same input power. The d-q axis current waves of the synchronous generator and the BDFIG were measured (Figure 3) by changing the input power at 8s.

As shown in Figure 3, the d-q axis current waves of synchronous generator and BDFIG almost coincided with each other, except a tiny difference at the point of change due to the neglection of the differentials.

4.2. Small-signal modelling for the VSC-BDFIG

The relationship between power angle and active power can be expressed as:

$$P_{e\_B} = \frac{E_{0\_B} U_p}{X_s} \sin\delta \tag{34}$$

where δ is the power angle, i.e. the electrical angle separating vectors e_{0_B} and up.

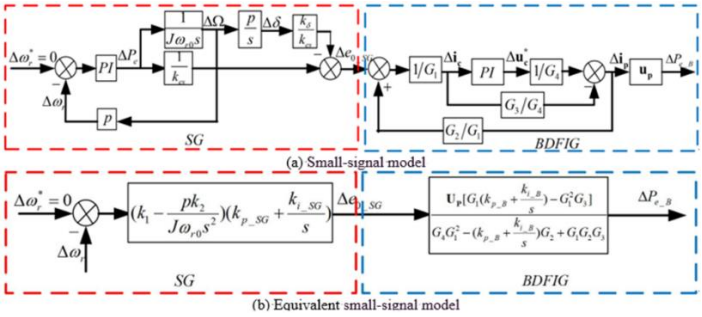

Figure 4. Small-signal model and equivalent small-signal model of the VSC-BDFIG

The relationship of i_c and i_p can be obtained from Reference [*] and the electric quantities of both generator are pu values. Thus, we have:

$$P_{e\_B} = \frac{E_{0\_B} U_p}{X_s} \sin\delta \tag{34}$$

where δ is the power angle, i.e. the electrical angle separating vectors e_{0_B} and u_p.

Then, we have:

$$\begin{aligned}\Delta P_{e\_B} &= \frac{U_{p0}\sin\delta_0}{X_s}\Delta e_{0\_B} + \frac{e_{0\_B}\sin\delta_0}{X_s}\Delta u_P + \frac{e_{0\_B}U_{p0}\cos\delta_0}{X_s}\Delta\delta \\ &= k_{es}\Delta e_{0\_B} + k_{Us}\Delta u_p + k_\delta\Delta\delta\end{aligned} \tag{35}$$

Taking the grid voltage as a constant, we have:

$$\Delta P_{e\_B} = k_{es}\Delta e_{0\_B} + k_\delta\Delta\delta \tag{36}$$

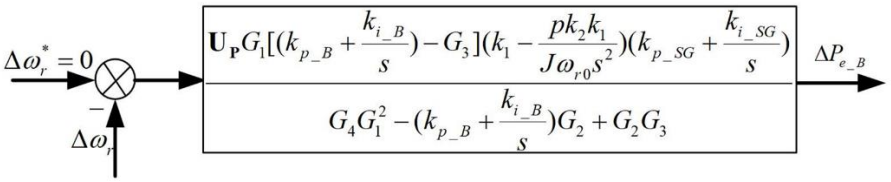

Figure 5. Simplest small-signal model of the VSC-BDFIG control system

The relationship of ic and ip can be obtained from Reference [*] and the electric quantities of both generator are pu values. Thus, we have:

$$u_c = G_3 i_c + G_4 i_p \tag{37}$$

where

$$G_3 = (\frac{L_{s2r}^2}{L_r} - L_c)[s + j(\omega_p - (p_1 + p_2)\omega_r)]$$

;

$$G_4 = \frac{L_{s2r}L_{s1r}}{L_r}[s + j(\omega_p - (p_p + p_c)\omega_r)]$$

$$G_4 = \frac{L_{s2r}L_{s1r}}{L_r}[s + j(\omega_p - (p_p + p_c)\omega_r)]$$

In this way, the small-signal model of the VSC-BDFIG was established (Figure 4(a)). The equivalent small-signal model of the VSC-BDFIG is given in Figure 4(b), which demonstrate that the BDFIG mimics all running features of the synchronous generator.

4.3. Stability analysis of the VSC-BDFIG

According to Figure 4, the VSC-BDFIG is composed of two parts: the synchronous generator in red box and the BDFIG in blue box.

The part of synchronous generator operated like an actual synchronous generator. The operation reflects the power variations with the speed. During the operation, the input active power of the BDFIG was the same as the synchronous generator. The inner potential obtained after the operation was consistent with that of the synchronous generator. When input power varied, the synchronous generator began to make

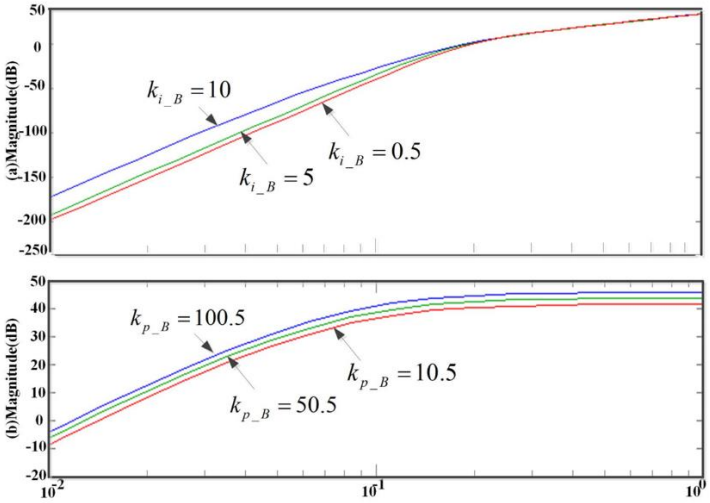

Figure 6. Stability effect of BDFIG parameters

adjustment, resulting in changes to the inner potential. Thus, it is possible to obtain ΔE_d and ΔE_q.

In the part of the BDFIG, the power winding is connected to the grid or load. The only controllable quantities are the d-q axis current waves of the control winding. The reference waves can be obtained by equation (28). Under the PI rule of inner currents, the actual control winding currents were in line with the reference waves. Hence, the mechanical motion of the BDFIG reflects its own physical properties, while the electrical motions are consistent with the reference. This means the parameters of these two parts can impact the stability of the VSC-BDFIG.

The simplest small-signal model of the VSC-BDFIG control system is displayed in Figure 5.

The relationship of $\Delta\omega_r$ and ΔP_{e_B} can be established as:

$$|M(s)| = \frac{u_p G_1[(k_{p\_B} + \frac{k_{i\_B}}{s}) - G_3](k_1 - \frac{pk_2k_1}{J\omega_{r0}s^2})(k_{p\_SG} + \frac{k_{i\_SG}}{s})}{G_4G_1^2 - (k_{p\_B} + \frac{k_{i\_B}}{s})G_2 + G_2G_3} \tag{38}$$

Next, the system stability was analysed in two phases with the parameters initialized as J=6.9， kp_B=100.5, k_{i_B}=10,k_{p_SG}=0.005 and k_{i_SG}=10.

4.3.1. Stability effect of BDFIG parameters

Figure 6 presents the amplitude-frequency curves of the inertial dynamics of the VSC-BDFIG at different k_{p_B} and k_{i_B}. As shown in Figures 6(a) and 6(b), the inner current loop parameters of the BDFIG exerted a major impact on the amplitude-frequency relation of magnitude |M(s)| in that the |M(s)| increased with k_{p_B} and k_{i_B} over a wide range of frequencies. Specifically, the effect of k_{i_B} concentrated in the low-frequency range, while that of k_{p_B} covered all frequencies. Thus, it is concluded that the explicit inertia of the VSC-BDFIG is positively correlated with the BDFIG parameters.

4.3.2. Stability effect of synchronous generator parameters

Three factors, namely, k_{i_SG}, k_{p_SG} and T_j , were analysed to disclose their impacts on same as (1). The resulting amplitude- frequency curves are displayed in Figure 7 below.

It can be seen from Figures 7(a) and 7(b) that the magnitude |M(s)| decreased with the growth of k_{i_SG} and k_{p_SG}. The impact of k_{i_SG} mainly emerged in the high-frequency range. When k_{i_SG} increased to 0.5, amplitude-frequency curve reached the peak, indicating the resonance appeared in the control system. By contrast, the impact of k_{p_SG} mainly emerged in the low-frequency the frequency features of |M(s)| at a certain operation point. The initial parameters are the range. According to Figure 7(c), the wind turbines manifested a relatively large inertia, which approached the integration constant T_j in active power control loop. This is because the grid is under high-frequency disturbances, with a small inertia for low-frequency grid disturbances. It is also learned that the T_j had a great influence on the frequency features of |M(s)|. Figure 7(c) shows that the increase of T_j substantially bolstered the magnitude |M(s)| for all frequencies. As a result, the explicit inertia of VSC-based wind turbine is positively correlated with the integration constant T_j in active power control loop increases, and negatively with the dynamic response speed of the controller.

5. Simulation and results analysis

This chapter verifies whether the proposed VSC-BDFIG can provide the desired inertial response against rapid change of grid frequency. The verification was realized through simulation on the frequency response of a single wind turbine at different controller parameters and operation conditions.

The simulation was carried out on a typical four-machine two-area system (Figure 8). The system has three 900MVA conventional generators (SG1, SG2 and SG3), two aggregated loads, and a BDFIG rated at 600MW (400 ×1.5MW). SG1 and SG2 belong to Area I where the load is connected to bus 7, while SG3 and BDFIG are in Area II where the load is connected to bus 8.

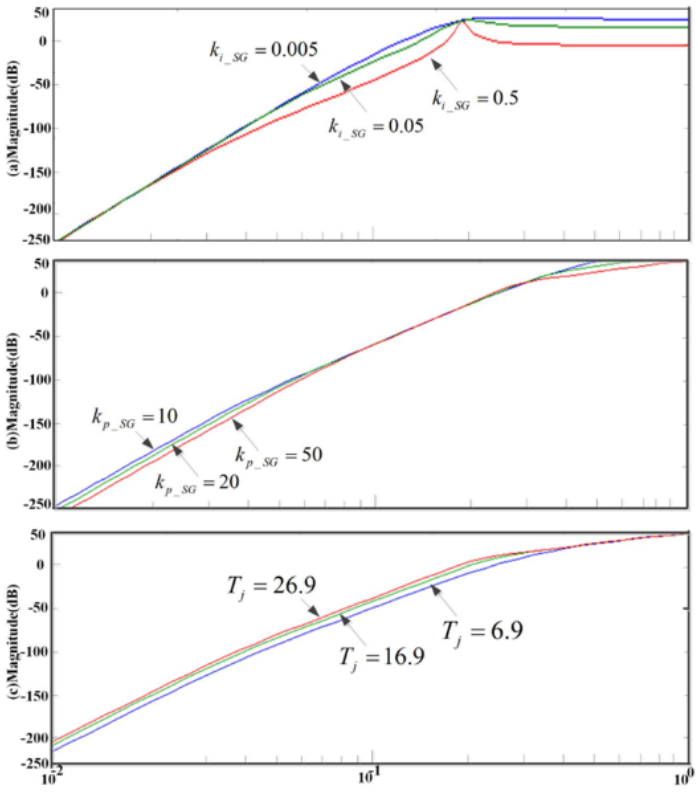

Figure 7. Stability effect of synchronous generator parameters

5.1. Effect of controller parameters

This subsection aims to disclose the impacts of controller parameters of the BDFIG and the synchronous generator. The short-circuit ratio of the test system was initialized as 4.0 in view of the access point of wind turbines and the sudden load increment (50 MW) was assumed to occur on bus 8 at 20s. Besides, the instantaneous penetration of wind power reached 18.1% in the initial state. The speed controller parameters were initialized as T_j = 6.9, k_{p_B} = 100.5 and k_{i_B} = 10 and taken as the reference values. The inertial responses of VSC-BDFIG at different controller parameters are displayed in Figure 9 below.

As shown in Figure 9 (a), the active power support capability was enhanced by the increase of k_{i_B} while other parameters remained unchanged. A possible reason lies in the increased impact of k_{i_B} on the current loop of the BDFIG (Figure 6(a)). In other words, the inner current loop responded rapidly to the increase of k_{i_B}, leading to the enhancement of the active power support capability.

Figure 9 (b) shows that the effect of k_{p_B} was similar that of the k_{i_B} , that is, the active power support capability increased with k_{i_B}. This is because the inner current loop reflects the speed of control winding current and the input of control winding current corresponds to the change in active power. Hence, the effect of parameters of the inner current loop on the active power support capability obeys the same trend as in Figure 9 (a).

It can be seen from Figure 9 (c) that the increase of T_j had a certain impact on the frequency response of wind turbines, which was obvious in the initial phase but diminished in the later phase of dynamic response. This trend is the result of the fact that T_j mainly affects the low- frequency features of the active power control loop, owing to the strong damping effect (i.e. the BDFIG has a large damping coefficient), but has little impact on the medium-frequency features. The medium-frequency features are the key determinant of the dynamic response of the active power control loop. Determined by the active power control, the explicit inertia of wind turbines is enhanced with the growth in T_j.

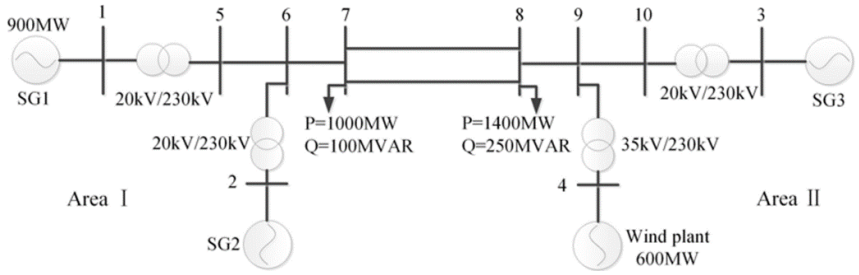

Figure 8. Test system

5.2. Response comparison

This subsection compares the dynamic responses of synchronous generator, vector control (VC)-BDFIG and VSC-BDFIG on the said test system (Figure 8). During the test, a sudden load increment (50MW) occurred on bus 8 at 5s. The power and frequency responses are recorded in Figures 10 and 11, respectively.

It is clearly seen from Figure 10 that the VSC-BDFIG provided an appreciable increase in output power like synchronous generator, as the maximum power surged up to 14% of the rated power, to alleviate the power shortage in the grid like synchronous generator. The positive contribution of the VSC-BDFIG is quite noticeable. By contrast, the VC-BDFIG acted as a constant-power source for the load

fluctuation, and made no positive contribution to supporting the grid frequency. As shown in Figure 11, it is evident that the system frequency change rate decreased significantly under the VC, and the minimum change rate belonged to SG1.

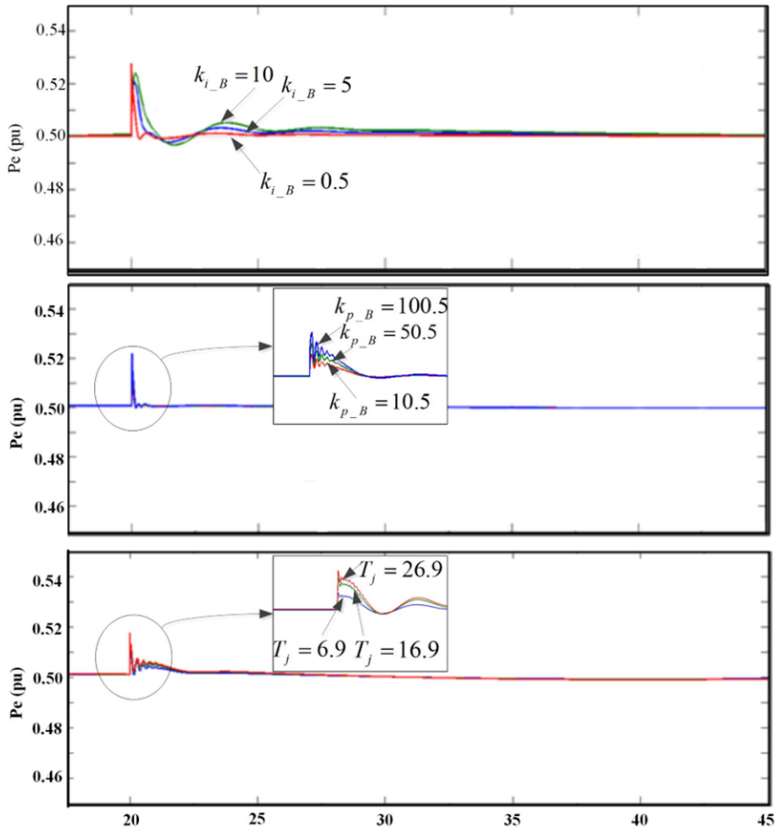

Figure 9. Inertial responses of VSC-BDFIG at different controller parameters

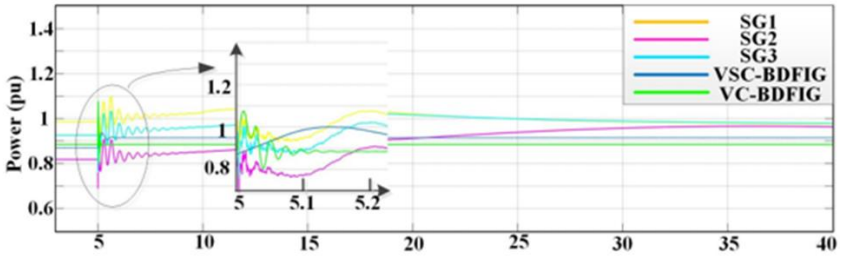

Figure 10. The sudden load power responses of SG1, SG2, SG3, VSC-BDFIG and VC-BDFIG

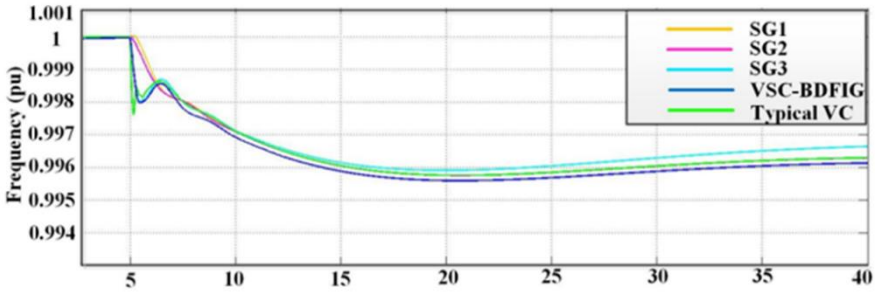

Figure 11. The sudden load frequency responses of SG1, SG2, SG3, VSC-BDFIG and VC-BDFIG

6. Conclusions

The virtual synchronous method is presented for the BDFIG-based WT referring to the well-known synchronization mechanism featured in SGs, which enables BDFIG-based WTs synchronize with power grid. More importantly, virtual synchronous control based BDFIG WTs can naturally provide the desired inertial response to undertake certain responsibility for the short-term frequency stability and meanwhile has good operation stability even when assessing weak grid.

In addition, the motion equation, on the basis of power imbalance between the input mechanical power and the output electromagnetic power, is introduced and used in the inertia characteristic analysis of WTs. The motion equation also makes the essential of WT's actual manifested inertia more clearly, which is actually controllable, frequency-dependent and synthetically affected by controller parameters and operating points. It should be particularly pointed out that the overall frequency response performance of WT is synthetically determined by the inertia and damping of WT's inner potential. In other words, large inertia does not mean the better response performance, which also depends on the system damping.

Acknowledgment

This work is supported by the Natural Science Foundation of China, No.51467018.

References

Ackermann T. (2005). *Wind Power in Power Systems.*

Arani M. F. M., EI-Saadany E. F. (2013). Implementing virtual inertia in DFIG-based wind power generation. *IEEE Transactions on Power Systems,* Vol. 28, No. 2, pp. 1373-1384. https://doi.org/10.1109/TPWRS.2012.2207972

EirGrid S. (2011). Ensuring a secure, reliable and efficient power system in a changing environment. *EIRGRID, SONI Report.*

Gorginpour H., Oraee H., Mcmahon R. A. (2013). A novel modeling approach for design studies of brushless doubly fed induction generator based on magnetic equivalent circuit. *IEEE Transactions on Energy Conversion*, Vol. 28, No. 4, pp. 902-912. https://doi.org/10.1109/TEC.2013.2278486

Jauch C., Cronin T., Sørensen P., Jensen B. B. (2007). A fuzzy logic pitch angle controller for power system stabilization. *Wind Energy*, Vol. 10, No. 1, pp. 19-30. https://doi.org/10.1002/we.205

Lv Z. P., Sheng W. X., Zhong Q. C. (2014). Virtual synchronous generators and its applications in micro-grid. *AProceedings of the CSEE*, Vol. 34, No.16, pp. 2591-2603.

Shuai Z., Shanglin M. O., Wang J., Shen Z. J., Tian W., Feng Y. (2016). Droop control method for load share and voltage regulation in high-voltage microgrids. *Journal of Modern Power Systems and Clean Energy*, Vol. 4, No. 1, pp. 76-86. https://doi.org/10.1007/s40565-015-0176-1

Solanki A., Nasiri A., Bhavaraju V., Familiant Y. L., Fu Q. (2016). A new framework for microgrid management: virtual droop control. *IEEE Transactions on Smart Grid*, Vol.7, No. 2, pp. 554-566. https://doi.org/10.1109/TSG.2015.2474264

Wang S., Hu J. B., Yuan X. M., Su L. (2015). On inertial dynamics of virtual-synchronous-controlled DFIG-based wind turbines. *IEEE Transaction on Energy Conversion*, Vol. 30, No. 4, pp. 1691-1702. https://doi.org/10.1109/TEC.2015.2460262